A Three Dimensional View of Velocity Using Lasers

James F. Meyers
NASA - Langley Research Center
Hampton, Virginia 23665

10th International Invitational Symposium
on Unification of Finite Element Methods
in Theory and Test
Worcester, Massachusetts
July 18-19, 1991

A Three Dimensional View of Velocity Using Lasers

by

James F. Meyers
NASA - Langley Research Center
Hampton, Virginia 23665

Abstract

The use of laser light sheet flow visualization, fringe-type laser velocimetry, and Doppler global velocimetry to make flow field investigations is described. The complementary nature of the techniques is demonstrated by using them to examine the vortical flow fields above a 75° swept delta wing and a YF-17 model in a low speed wind tunnel. The characteristics of these systems are described and their capability to provide fundamental velocity databases for CFD validation is assessed.

Introduction

The classic method of aircraft design begins by using fundamental aerodynamics and experience to create a design on paper. A model based on this design is then constructed and tested in a wind tunnel. The acquired force and balance data are studied and the model modified to bring the aerodynamic performance closer to the desired design goals. The model is then retested and the new results studied. This iteration continues until the design engineer is satisfied with the model performance. Finally, a full size prototype is built and flown to determine if the performance characteristics of the wind tunnel model are maintained in flight.

The development of modern aircraft utilizing vortex lift and other complicated flow fields to increase performance pushes the associated aerodynamics to the edge of stability. The ability of electronic fly-by-wire technology to instantly return the aircraft to stable flight from unstable excursions cannot be easily modeled using the classic approach. Force and balance testing must be supplemented by theoretical predictions of the flow fields and their experimental verification by off-body measurements. Computational fluid dynamics (CFD) is becoming increasingly sophisticated and has successfully predicted many classic flow fields. However, this technology is being

expanded to predict flows that have not or can not be measured with classic instrumentation. If the extrapolation continues without experimental verification, the value of their predictions quickly becomes questionable. The burden now shifts to the experimentalist and the instrumentation engineer to develop new measurement techniques that can provide experimental databases for code validation and the direct measure of flow field / airframe interactions.

The advent of the laser has provided the instrumentation engineer with a tool that serves as the basis for several new instrumentation systems. Fanning the laser beam into a light sheet provides a visualization of the flow field with greater capability and flexibility than classic shadowgraphy. The coherent characteristic of laser light is used as the basis for laser velocimetry, a nonintrusive, velocity measuring technique capable of measuring time dependent, three component velocity flow fields with accuracies better than 0.5 percent. Finally, these two ideas are now being combined in a new technique, Doppler global velocimetry, which provides simultaneous three-component velocity measurements within a desired measurement plane in real time.

Baseline Aerodynamic Investigation

The best way to illustrate the capabilities of these new laser based instrumentation systems is to use each to investigate the same flow field. The flow chosen is the classic leading edge vortex flow field above a delta wing. This selection is appropriate since the fundamental flow is utilized in many high performance aircraft designs to increase the flight performance envelope. A leading edge vortex pair contains a great deal of energy which, if carefully controlled, can provide significant lift on an aircraft. However, if a vortex is disturbed it will burst, dissipating its energy in a random manner resulting in a sudden loss of lift. This problem is of special concern for aircraft stability when only one vortex of a coupled pair bursts, resulting in sudden substantial rolling moments being applied to the aircraft. A classic vortex pair flow field was generated using a 75° delta wing, reference 1. The effects on the classic vortical flow field by external influences were determined using a model of a high performance aircraft which obtains much of its performance capabilities using vortex lift—the Northrop YF-17, reference 2.

Test Facility

While a vortex flow field is very stable, its characteristics are easily affected by external influences. Thus the wind tunnel flow should be stable with a constant freestream velocity and low turbulence during the time period required to conduct the flow field investigation. The Basic Aerodynamic Research Tunnel, reference 3, was designed to provide such a stable platform. The primary function of the facility is to use state-of-the-art instrumentation systems to fully investigate and document fundamental aerodynamic flow fields. These investigations will establish the experimental databases necessary for the development and verification of generalized computational fluid dynamic computer codes. The facility, shown in figure 1, is an open circuit tunnel that has a test section measuring 0.71 m high, 1.02 m wide and 3.05 m long. The test section is divided into two 1.524 m long bays. The maximum flow velocity in the test section is 67 m/sec which yields a Reynolds number of 4.6×10^6 /m. The airflow entering the test section is conditioned by a honeycomb, four anti-turbulence screens and an 11:1 contraction ratio. The 0.1 m thick honeycomb has a 0.01 m cell size. The screens are 7.87 mesh per centimeter with a porosity (ratio of open area to total area) of 64 percent. These flow conditions coupled with an excellent fan speed controller, provide a low-turbulence, uniform flow in the test section. The longitudinal component of turbulence intensity (measured with a hot wire) varies from approximately 0.05 percent for a tunnel q (dynamic pressure) of 4.13 N/m^2 (V_∞ = 28 m/sec) to 0.08 percent for a q of 18.6 N/m^2 (V_∞ = 59.4 m/sec).

The laser techniques require particles to be embedded within the flow to provide the scattering centers necessary to make measurements. A vaporization/condensation generator using propylene glycol provided the seeding particles for laser light sheet flow visualization and subsequently for velocity measurements using the Doppler global velocimeter, reference 3. The particle size distribution of propylene glycol drifting through the test section (tunnel off) is shown in figure 2. When the flow is adjusted to a q of 3.47 N/m^2 (V_∞ = 25.6 m/sec), the propylene glycol begins to evaporate, yielding the particle size distribution shown in figure 3. Polystyrene particles, 0.8 microns in diameter, suspended in 100-proof ethanol were injected into the flow upstream of the honeycomb using an agricultural spay nozzle, references 1 and 2, to provide the seeding particles for the laser velocimeter. Upon leaving the spray nozzle the ethanol evaporated, leaving the polystyrene particles to follow the flow. The spray nozzle (or the ejection nozzle from the vaporization/condensation generator) is mounted on a computer-controlled 2-axis traverse system which allows remote positioning of the particle plume.

Laser Light Sheet

Typically a laser light sheet is generated using a powerful continuous wave laser such as an Argon ion and a cylindrical lens or glass rod to spread the beam into a thin sheet. Although this approach is quite simple, it is difficult to place the sheet in an arbitrary plane to obtain various views of the flow field. Using a twin-mirrored galvanometer to rapidly move the reflected light beam, the system can be operated in a variety of modes and provides either single or simultaneous multiple light sheets. The system can also rotate the sheet through 360 degrees about the optical axis. The laser light sheet generating equipment is shown in figure 4.

Laser Velocimeter

The laser velocimeter is an orthogonal three component fringe type system using orthogonal collection of the scattered light to minimize sample volume size and allow close approach to unprepared models. The system, shown in figure 5, uses the 496.5, 476.5, and 514.5 nm wavelengths from an Argon ion laser to measure the streamwise (u), vertical (v), and cross tunnel (w) velocity components, respectively. The transmission optical system for the u and v components is located on the side of the test section with the receiving optical system located above the test section slightly off-perpendicular (15°) toward the upstream direction. The transmission optical system for the w component is placed above the test section perpendicular to the u-v optical axis. Its receiving optical system is adjacent to the u-v transmitter, rotated 15° downstream about the sample volume. This configuration yields a very small spherical sample volume, 140 microns in diameter, and reduces the amount of scattered light or flare from the model surface entering the collecting optical system. The sample volume can be placed within 70 microns from the unprepared model surface before flare reduces signal-to-noise below acceptable limits for the signal processing electronics. Bragg cells are used in each component to provide full measurement directionality. A photograph of the laser beams crossing over the 75° swept delta wing model is shown in figure 6.

The optics and laser move as a unit on a traversing system that provides 1 meter of travel, with 10 micron resolution in all three axes. The design of the traverse system provides flexibility in optical mounting and allows the optics to be remounted in forward scatter or 180° backscatter configurations should the test require. As shown in figure 5, the traversing system completely surrounds the test section to maximize system stability.

The photomultiplier output from each component is processed by high-speed burst counters utilizing 500 MHz clocks. The processed signals are acquired by a high-speed, parallel data acquisition unit, reference 4. This unit provides the timing circuits to measure the interarrival times between successive particle velocity measurements in each component. These times are used to remove any statistical bias present in the measurement ensemble. Each component, interarrival time circuit and auxiliary channel contains 64k words of data storage. Once the measurement at a point is completed, the acquired data is then passed to the system minicomputer for statistical processing and data storage.

Doppler Global Velocimeter

Laser light sheet flow visualization uses a standard video camera to view the scattered light from particles passing through the sheet. The flow structure is visualized through changes in scattering intensity caused by spatial and temporal variations in particle number density induced by the flow field. The scattered light also contains another property—it is shifted in optical frequency due to the Doppler effect brought about by the motion of the particles passing through the sheet. If this shift can be measured, the velocity field within the plane defined by the light sheet can be determined. The Doppler global velocimeter uses the edge of an absorption line in molecular Iodine to serve as a frequency discriminator to directly measure the Doppler shift of the collected scattered light, reference 5. The Argon ion laser operating in single-line mode at 514.5 nm is tuned by tilting the intercavity etalon to an optical frequency corresponding to a point midway along the edge of an absorption line of an Iodine absorption line filter (ALF), figure 7. Collected scattered light from a stationary object or cloud of particles will be attenuated by 50 percent as it passes through the ALF. If the object or particle cloud is moving, the attenuation through the ALF will increase (or decrease, depending on the direction of movement) by an amount proportional to the Doppler shift. By using the ALF as a filter for the camera, the entire laser light sheet can be viewed and the velocity field determined.

In practice, particle size distribution and number density, and the laser light sheet intensity profile are other factors influencing the amount of collected scattered light reaching the viewing camera. These influences can be minimized by viewing the same scene with a second camera without an ALF, figure 8, to provide a reference signal used to normalize the viewing camera output. The two cameras must be aligned with corresponding pixels in each camera viewing the same portions of the light sheet. Other influences from nonuniform optical elements and variations in pixel sensitivities in the CCD cameras are removed using

pixel-by-pixel ratio calibrations. A view of the Doppler global velocimeter viewing the vortical flow above the delta wing in the tunnel is shown in figure 9.

Investigation of the Flow Field Above the Delta Wing

The first series of tests using these three techniques is the investigation of the vortical flow field above a 75° swept delta wing. The model has a 0.305 meter span and sharp leading edges (10° bevel on the lower surface with the upper surface flat). An angle of attack of 20.5° yields a stable vortex flow above the model. An increase to an angle of attack of 40.0° yields burst vortices. The tunnel speed was adjusted to obtain a chord Reynolds number of 1.0 million for both conditions. The laser velocimeter and Doppler global velocimeter investigations were conducted in a plane orthogonal to the surface of the model at an $x/L = 0.7$.

Using the laser light sheet, the vortices are clearly seen above the model at an angle of attack of 20.5°, at the $x/L = 0.7$ location in figure 10. Rotating the light sheet to be parallel with the centerline of the vortices, the core region is visualized, figure 11. Increasing the angle of attack causes the right vortex to burst while the left remains intact, figure 12. This asymmetry may be caused by a known 0.2° roll in the model. Changing the laser to a pulsed doubled YAG, the visualization brings out fine details in the vortical flow including eddy circulation about the main core, figure 13. A repeat of figure 12 using this laser is shown in figure 14.

The three component mean velocity measurements, reference 1, obtained with the laser velocimeter at an angle of attack of 20.5° are shown in figure 15 and at 40.0° in figure 16. It is noted that the streamwise component increases to twice freestream velocity within the core of the vortex, but reverses when the vortices burst. The angular motion seems to change little in either case. The normalized standard deviations for the streamwise component at an angle of attack of 20.5°, figure 17, indicate a high level of velocity fluctuations. These findings appear to conflict with the flow visualization results which show very stable vortices. Using the Doppler global velocimeter to measure the entire vortical flow, reference 6, every 33 msec instead of the 8 hours required by the laser velocimeter, the solution may be found.

The Doppler global velocimeter was configured to measure the flow velocity 26.5° from the streamwise direction within the horizontal plane, figure 8. A single frame, shown in figure 18, clearly shows the vortical flow with the expected velocity pattern. The velocity at the top

of the left vortex should match the bottom of the right with the flow next to the wing being slightly higher due to flow compression. The top of the right should likewise match the bottom of the left. A velocity profile through the center of the vortices, shown in figure 19, is easier to visualize than the gray scale image in figure 18. In calculating the average from several frames to obtain the required information to remove pixel sensitivity variations from the data, the velocity profiles were found to vary as much as 15 percent from frame to frame. These changes were not random in location, but a general change in the entire vortex. Not understanding the reason for these variations, the real time analog video was viewed. The video showed a stable vortex flow field with the variations in velocity indicated by the laser velocimeter measurements. That is, until the video was played in slow motion. The vortex was very stable with little turbulence; however, every ten frames an entire vortex would increase velocity indicating a surge in flow. The two vortices did not surge together, but oscillated in a phased pattern.

Vortical Flow Above a YF-17 Model

The flow field measurements above the delta wing were part of an investigation to provide general knowledge about vortex flow fields and establish a measurement database for verification of computational fluid dynamics computer codes. This investigation also served as a preliminary test to determine the characteristics of the optical measurement systems on vortical flows before investigating the complicated flow above a model configuration. The final goal of the program conducted by Sellers, Meyers, and Hepner, reference 2, was to investigate the flow above a YF-17 model to determine the vortex interaction with the vertical stabilizers.

Modern fighter aircraft at high angles of attack generate vortices which produce substantial increases in lift. The vortices are shed by the sharp wing leading edges, slender fuselage forebodies, and by the high-swept wing leading-edge extensions (LEXs). There is also interest in techniques which exploit the vortices to provide increases in maneuverability in the high angle of attack regime where conventional control surfaces lose their effectiveness, reference 7. Figure 20 is a photograph of an F-18 aircraft at high angle of attack and shows the LEX vortices made visible with a smoke bomb.

The interaction of the vortices with the tail surfaces can cause structural problems. Both the F-15, reference 8, and the F-18, reference 9, have encountered buffeting and/or structural fatigue problems with the vertical tails at high angles of attack. The buffeting is due in a large part to the breakdown of the vortices ahead of the tails.

Vortex bursting or breakdown is meant to describe the condition where the axial velocity at the core of the vortex abruptly stagnates followed by a rapid expansion of the vortex core. After the expansion, the flow changes to a highly-turbulent swirling state.

The lack of quantitative flow field data has hampered efforts to develop theoretical methods to predict aircraft buffet or a buffet design criteria for the high angle of attack flight regime. There have been numerous research papers written on the subject of vortex flows from slender delta wings, but much of this data is of limited use since the instrumentation that was available at the time was not capable of measuring the velocity field in a burst vortex. Flow field data above configurations are even more scarce.

The model was a Northrop YF-17 configuration which was the prototype for the McDonnell Douglas F/A-18 Hornet. The YF-17 shown in the three-view sketch in figure 21 incorporates design features that are typical of many of the current generation fighter aircraft. It includes a moderately-swept (26.6°) wing, twin vertical tails, and a highly-swept (80°) leading edge extension. The flow field generated by this aircraft exhibits many of the characteristics of the present generation fighter aircraft, as well as the problems such as vortex interaction with the tail surfaces.

All data were obtained at a free stream dynamic pressure of 12.4 N/m^2, which represents free stream velocities of 48.5 m/sec. This speed results in test Reynolds numbers of 326,000 based on the mean aerodynamic chord. The two angles of attack, 15° and 25°, investigated represented conditions where the vortices over the model would be unburst and burst, respectively. The higher angle of attack represented a condition where, based on Northrop YF-17 flight test data, the tail buffet loads increase significantly, The two survey stations, 440 and 524, where flow field data were obtained are shown in figure 21. Velocity measurements were acquired over the right half of the model.

Flow visualization of the two measurement planes are shown in figure 22 for 15° angle of attack. The corresponding laser velocimeter mean velocity measurements for stations 440 and 524 are shown in figures 23 and 24, respectively. The cross flow vectors clearly show the LEX vortex is positioned outboard of the vertical tail and close to the wing upper surface. The spanwise component of velocity has accelerated to approximately 90 percent of freestream directly under the LEX vortex. The streamwise component of velocity in the core of the LEX vortex has decelerated to approximately 80 percent of freestream. The flow separates at the leading edge of the wing at this angle of attack. There is a large separated flow region over the outer wing panel at these

stations. There are reversed flows of up to 10 percent of freestream in the streamwise velocity component over the outer third of the wing span. The LEX vortex had the favorable effect of preventing flow separation over the inboard portion of the wing.

The flow field takes on a dramatically different character at 25° angle of attack. The flow visualization results are shown for the two measurement stations in figure 25. The mean velocity vectors and contours are shown in figures 26 and 27 for stations 440 and 524, respectively. The cross flow velocity vectors show that the wing separation region and the LEX vortex have grown in size and the LEX vortex is positioned directly in line with the vertical tail. The LEX vortex has burst at the 440 station at this angle of attack. The core of the LEX vortex magnifies at the 524 station and contains a large area of reversed flow as shown in figure 27. The reversed flow reaches a maximum of approximately 10 percent freestream. Although the LEX vortex has burst, there is still a structured swirling pattern around the vortex. This is consistent with the measurements of a burst vortex over the 75° delta wing, figure 16; however, the flow field is more complicated due to the presence of the wing separation which has merged with the flow from the LEX vortex. The region of reversed flow in the wing separation region has grown in both size and strength, with the magnitude of the reverse flow increasing to approximately 20 percent of free stream.

The standard deviation of velocity provides a measure of the intensity of the fluctuating input forcing the vertical tail to vibrate. The standard deviation is nondimensionalized by the freestream velocity to provide a measure of the relative turbulence intensity. The normalized standard deviation for the streamwise, vertical and spanwise components are shown in figures 28, 29, and 30, respectively, for the 524 station at an angle of attack of 25°. The maximum value for the normalized standard deviation reaches levels of approximately 0.40, 0.35, and 0.30 for the streamwise, vertical and spanwise components, respectively. Along with being large values, the regions of influence are quite large. The large standard deviations in the upper portion of the wing separation region are due to movement of the shear layer through the measurement location.

Summary

Laser light sheet, fringe-type laser velocimetry, and Doppler global velocimetry have been described and used to investigate the vortical flow field above a delta wing and a YF-17 model. It has been shown that using only one technique will yield insight into the fluid mechanics of

the flow, but leaves many unanswered questions. Adding the other two complementary measurement techniques greatly increases the understanding of the flow. Laser light sheet visualization quickly gives an overall view of the flow field, and if a pulsed laser is used, can show small flow structures that are averaged out with slower techniques. Fringe type laser velocimetry can be used to obtain three component mean velocity and higher statistical measurements at points within the flow. The fine accuracy of the technique provides detailed investigations of the flow that can be used to develop the measurement databases necessary to verify computational fluid dynamic computer codes. The Doppler global velocimeter provides the real time aspect of flow visualization while affording measurements of velocity. Although this new technique will require development to match the accuracy of the fringe-type laser velocimeter, it will provide real time, three component velocity measurements simultaneously over an entire measurement plane.

References

1. Meyers, J. F.; and Hepner, T. E.: *Measurement of Leading Edge Vortices from a Delta Wing Using a Three Component Laser Velocimeter*. AIAA 15th Aerodynamic Testing Conference, San Diego, California, paper AIAA-88-2024, May 18-20, 1988.

2. Sellers, W. L., III; Meyers, J. F.; and Hepner, T. E.: *LDV Surveys over a Fighter Model at Moderate High Angles of Attack*. SAE 1988 Aerospace Technology Conference & Exposition, Anaheim, California, October 3-6, 1988.

3. Sellers, W. L., III; and Kjelgaard, S. O.: *The Basic Aerodynamics Research Tunnel—A Facility Dedicated to Code Validation*. AIAA 15th Aerodynamic Testing Conference, San Diego, California, paper AIAA-88-2024, May 18-20, 1988.

4. Cavone, A. A.; Sterlina, P. S.; Clemmons, J. I., Jr.; and Meyers, J. F.: *A High-Speed Buffer for LV Data Acquisition*. Proceedings of the International Congress on Instrumentation in Aerospace Simulation Facilities, College of William and Mary, Williamsburg, Virginia, pp. 113-119, 1987.

5. Komine, H.; Brosnan, S. J.; Litton, A. B.; and Stappaerts, E. A.: *Real-Time, Doppler Global Velocimetry*, AIAA 29th Aerospace Sciences Meeting, Reno, Nevada, paper AIAA-91-0337, January 7-10, 1991.

6. Meyers, J. F.; and Komine, H.: *Doppler Global Velocimetry—A New Way to Look at Velocity*, ASME Fourth International Conference on Laser Anemometry, Cleveland, Ohio, August 23-27, 1991.

7. Murri, D. G.; and Rao, D. M.: *Exploratory Studies of Actuated Forebody Strakes for Yaw Control at High Angles of Attack*, AIAA Atmospheric Flight Mechanics Conference, paper AIAA-87-2557, Monterey, California, August 1987.

8. Triplett, W. E.: *Pressure Measurements on Twin Vertical Tails in Buffeting Flow*, Journal of Aircraft, Vol. 20, No. 11, November 1983.

9. Wentz, W. H., Jr.: *Vortex-Fin Interaction on a Fighter Aircraft, AIAA 5th Applied Aerodynamics Conference*, paper AIAA-87-2474, Monterey, California, August 1987.

Figure 1.- Basic Aerodynamic Research Tunnel (BART).

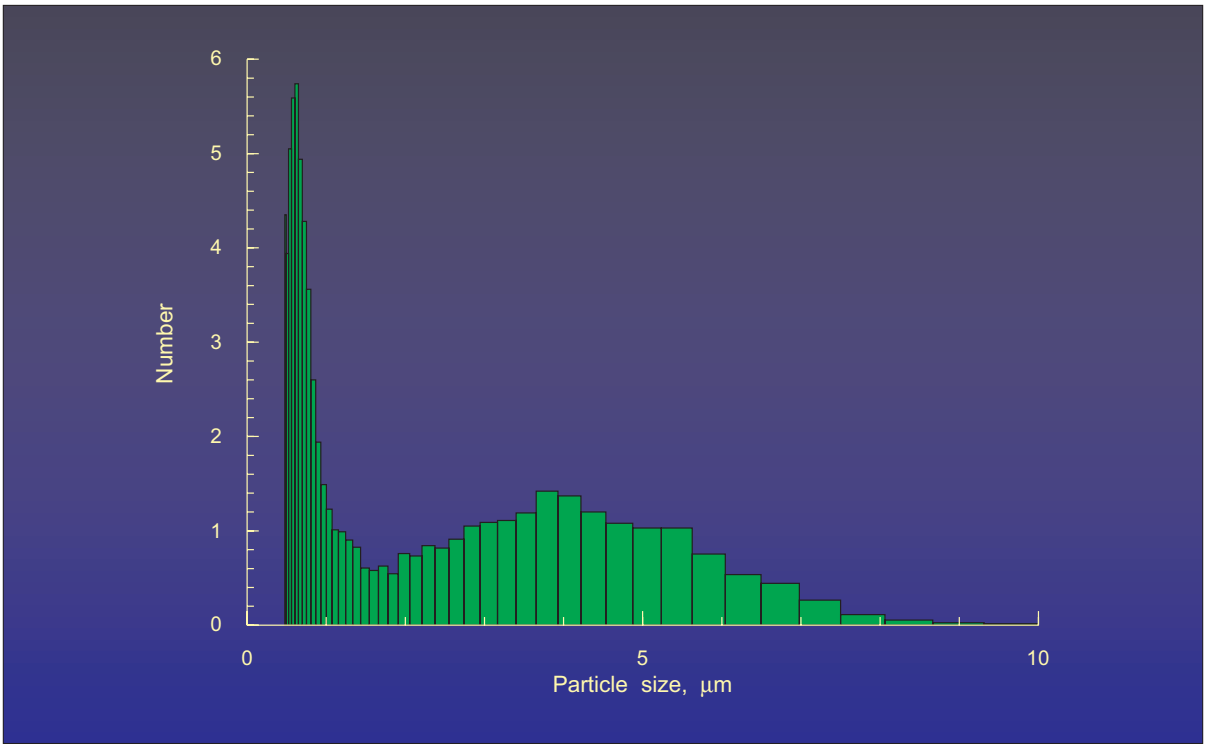

Figure 2.- Particle size distribution of propylene glycol from a vaporization / condensation generator, tunnel q = 0 N/m^2.

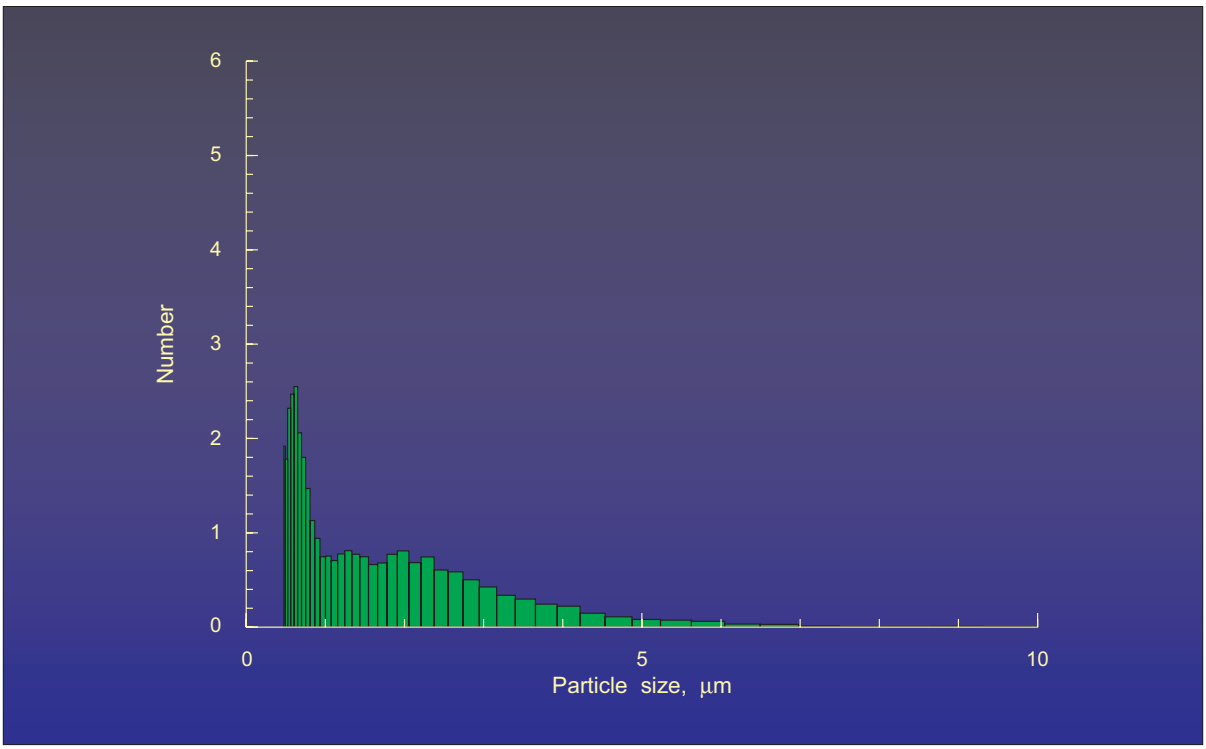

Figure 3.- Particle size distribution of propylene glycol from a vaporization / condensation generator, tunnel q = 3.47 N/m^2.

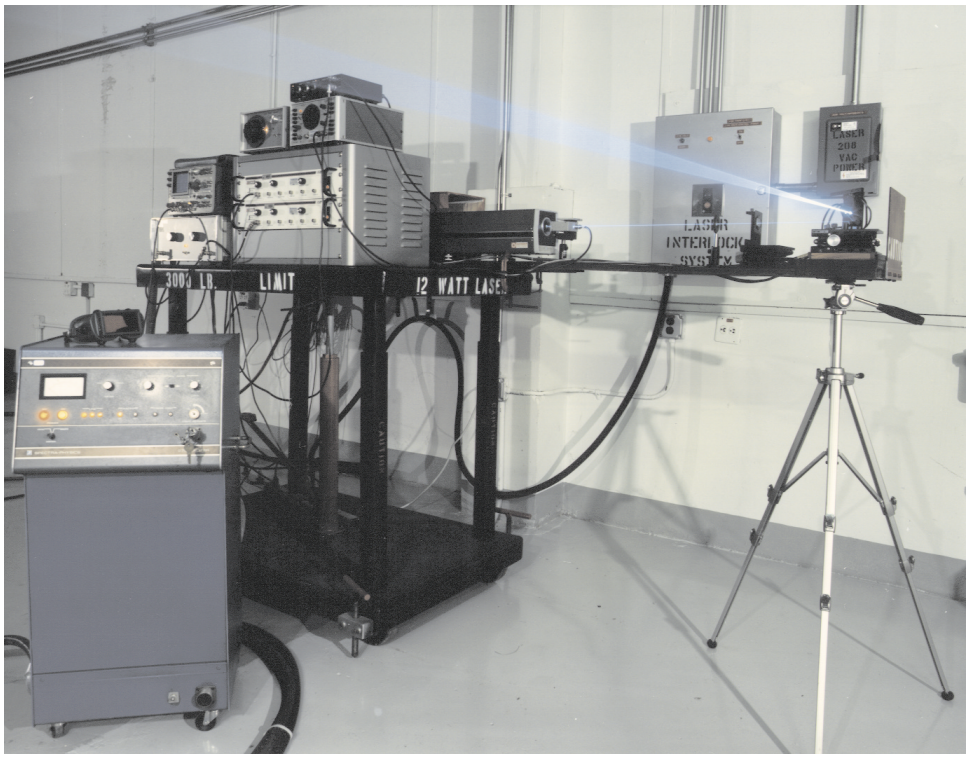

Figure 4.- Argon ion laser and twin-mirrored galvanometer laser light sheet system.

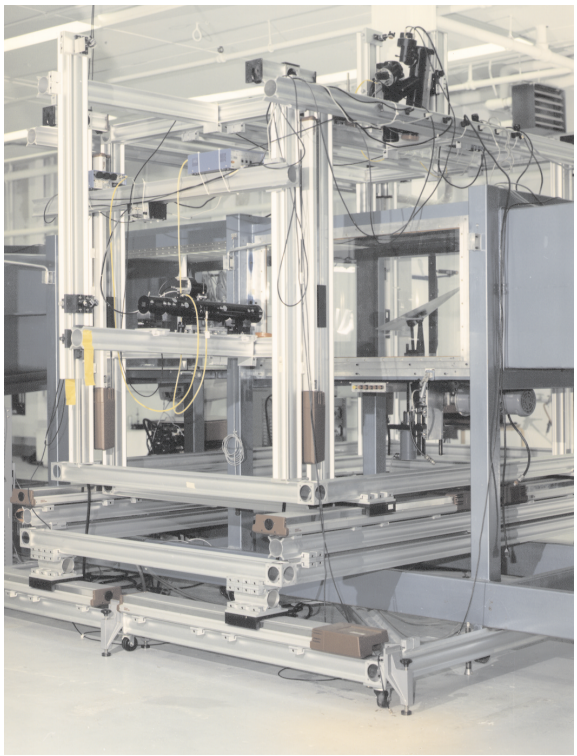

Figure 5.- The orthogonal three component laser velocimeter system mounted on the traversing system.

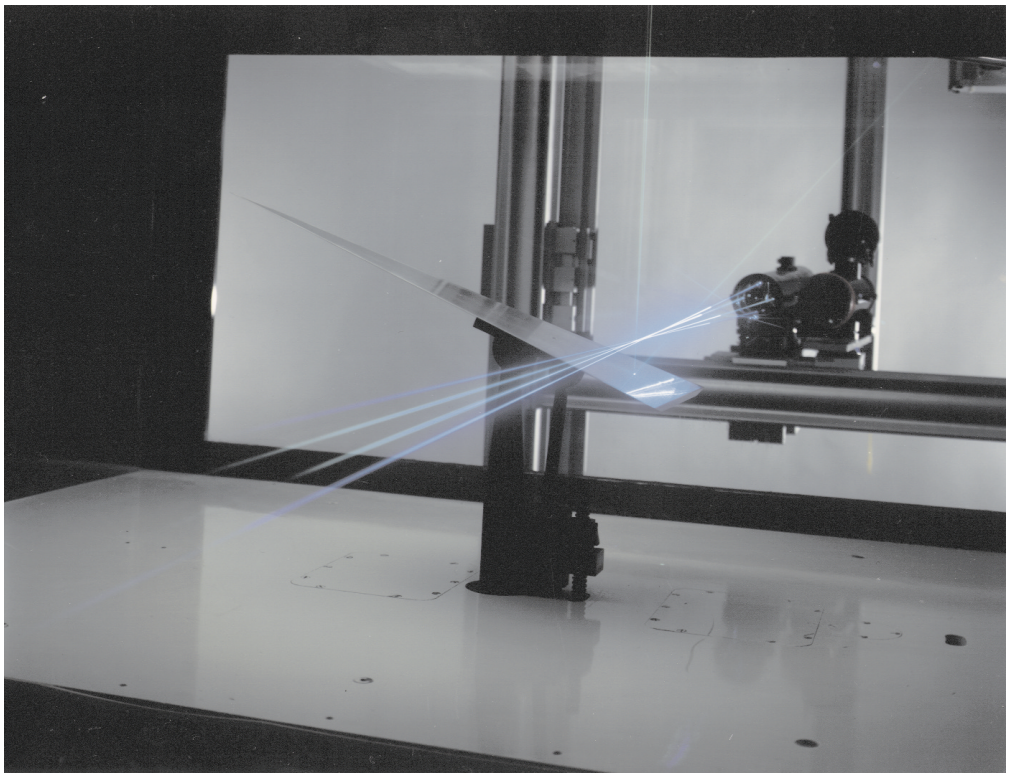

Figure 6.- View of the 75^{o} delta wing in BART with the crossing laser beams from the orthogonal three component laser velocimeter.

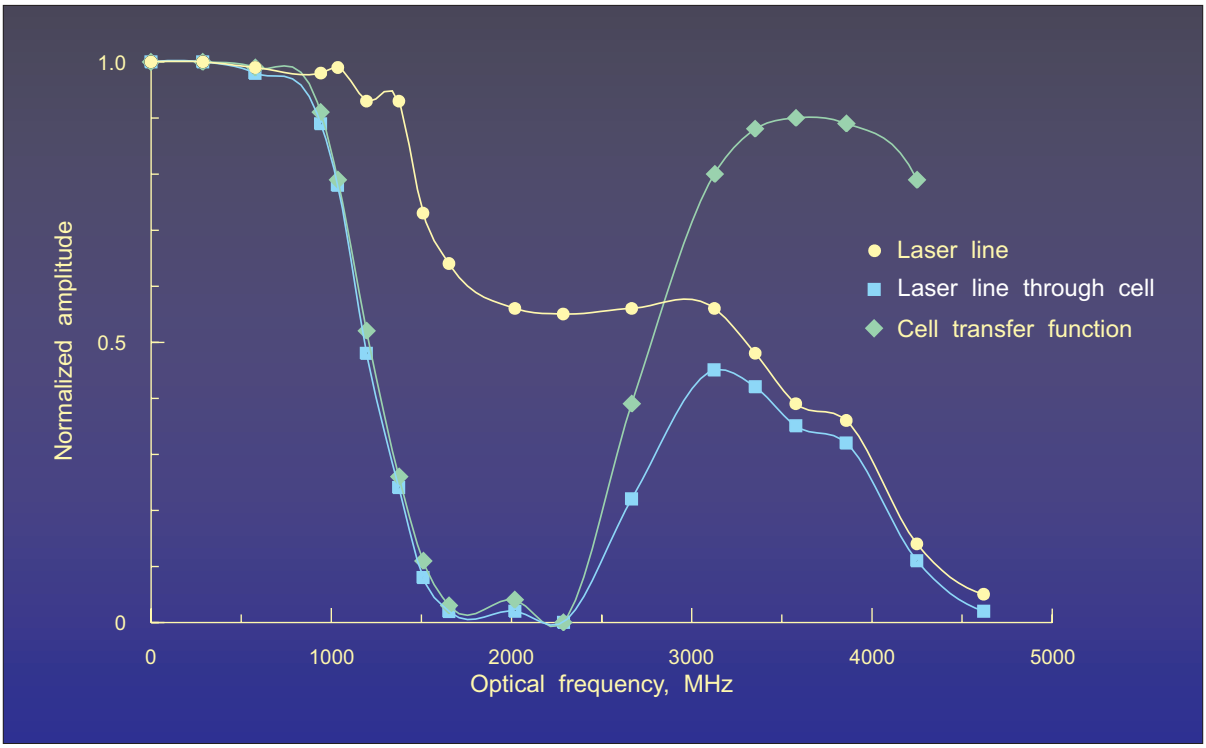

Figure 7.- Transfer function of the Iodine absorption line filter, ALF.

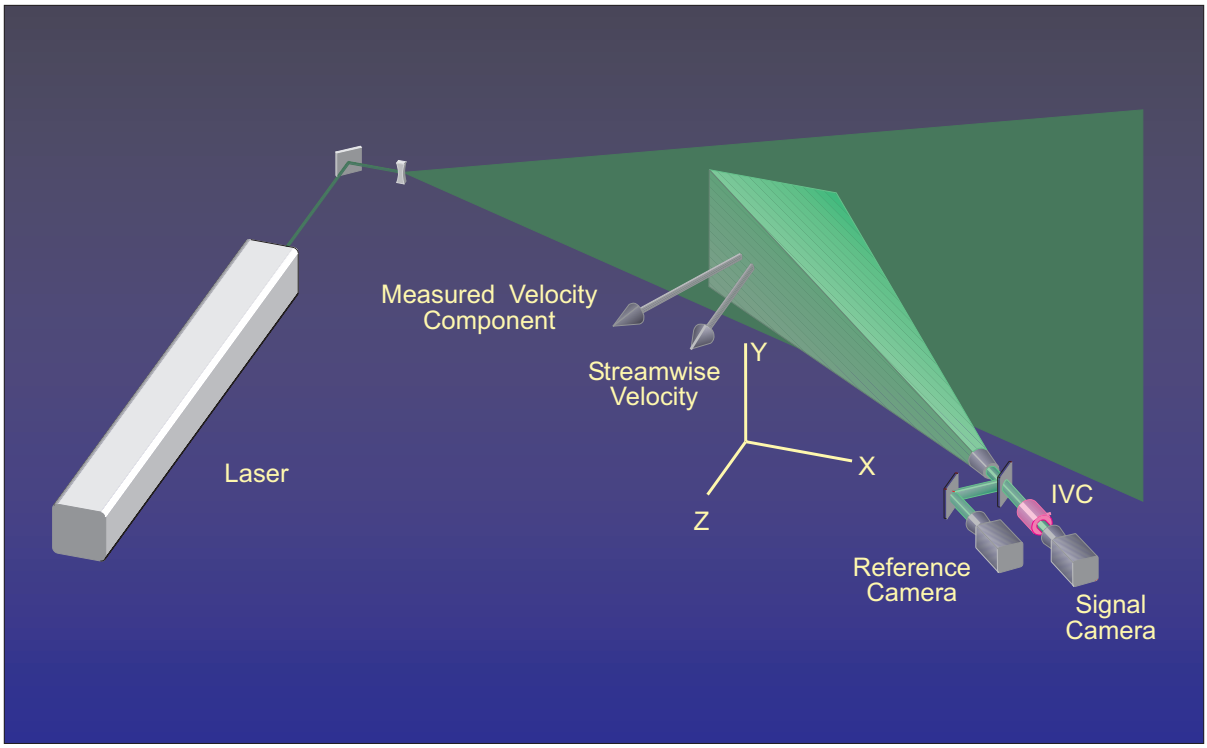

Figure 8.- Graphical representation of the Doppler global velocimeter in BART.

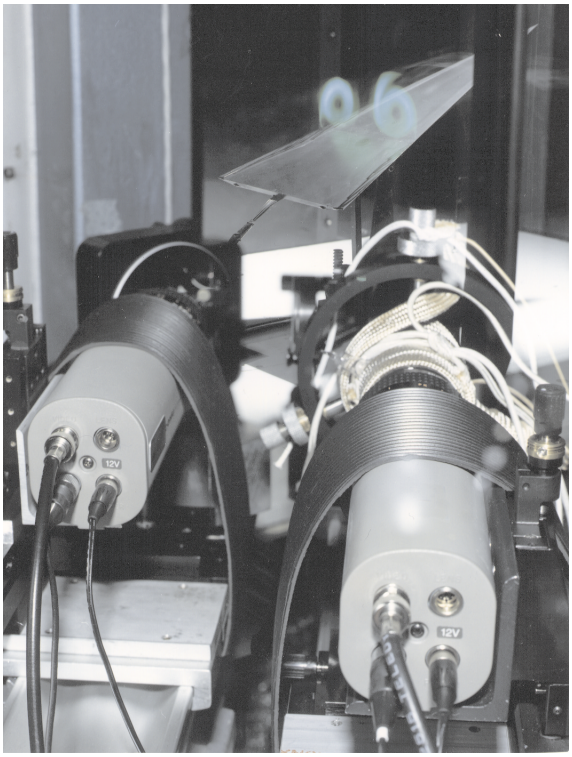

Figure 9.- Photograph overlooking the receiving optical system of the Doppler global velocimeter to view the laser light sheet illuminated vortex flow field above a 75^{o} delta wing.

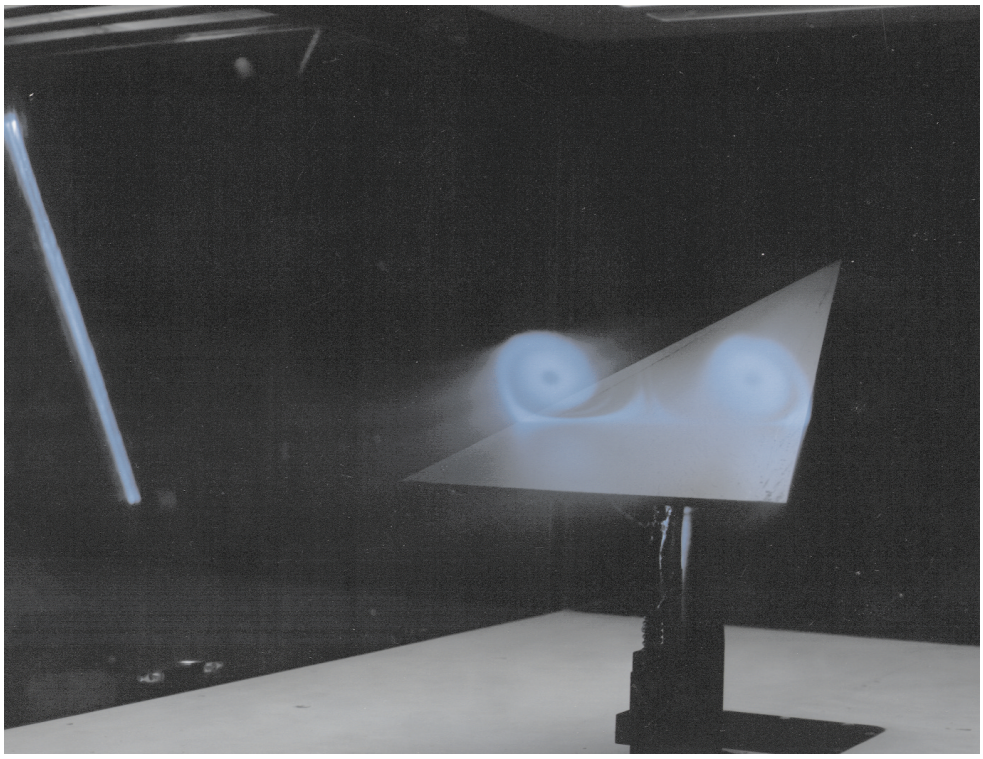

Figure 10.- Laser light sheet flow visualization of the vortex flow above the 75^{o} delta wing at an angle of attack = 20.5^{o}.

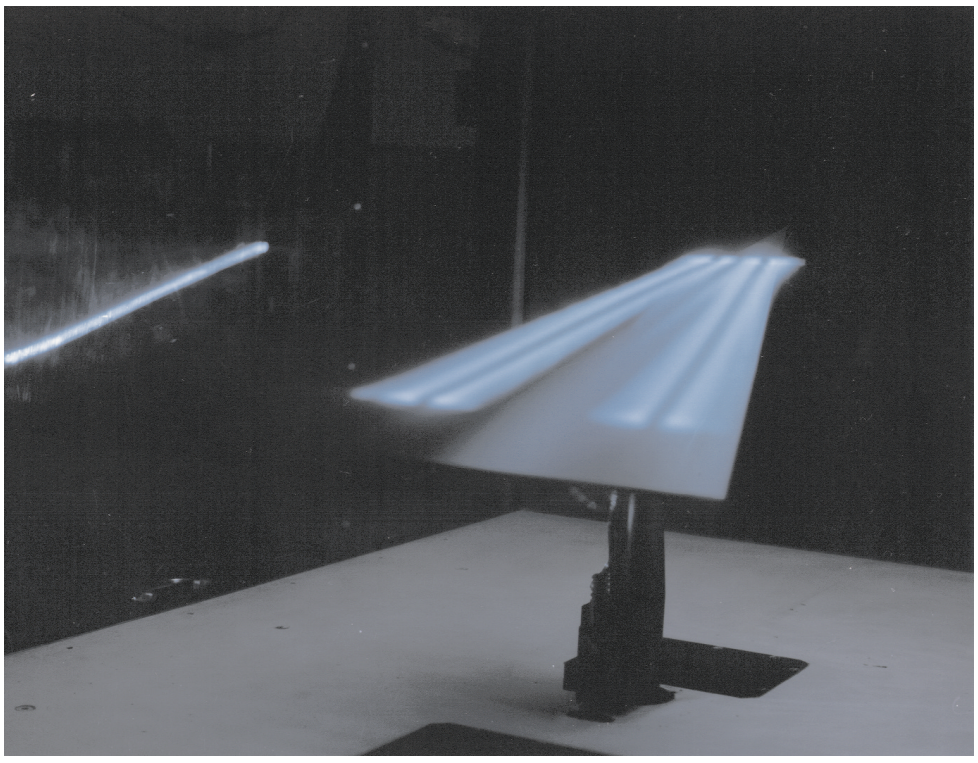

Figure 11.- Laser light sheet flow visualization of the vortex flow with the sheet orientated in the plane of the two vortices - unburst condition.

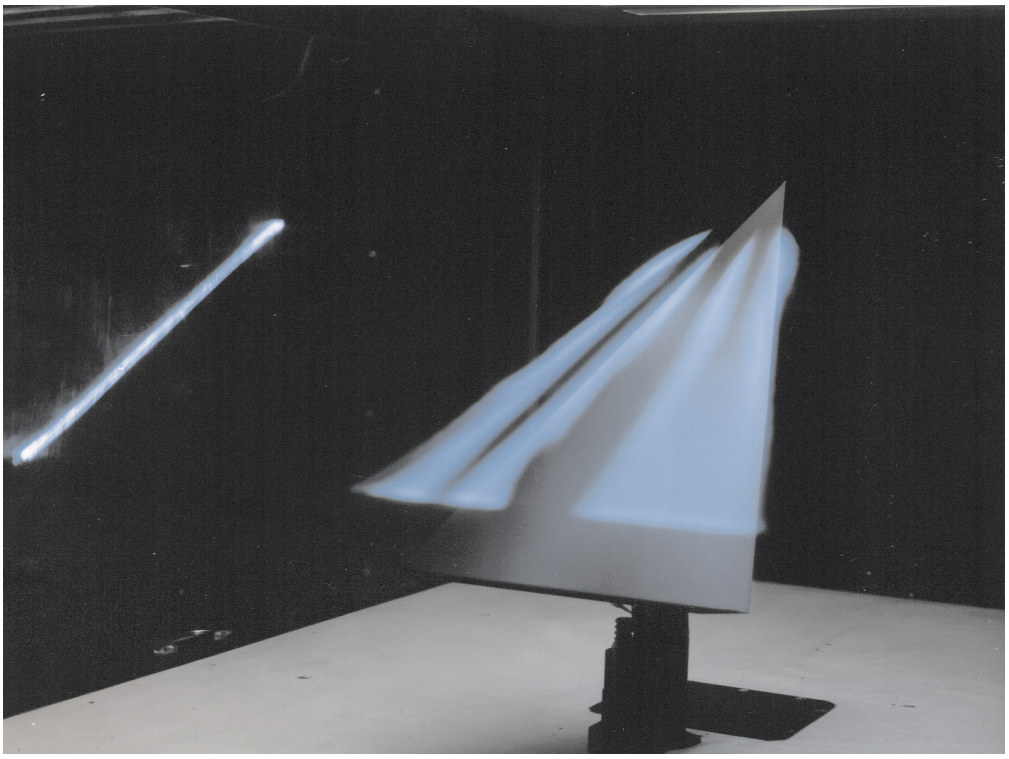

Figure 12.- Laser light sheet flow visualization of the vortex flow with the sheet orientated in the plane of the two vortices - burst condition.

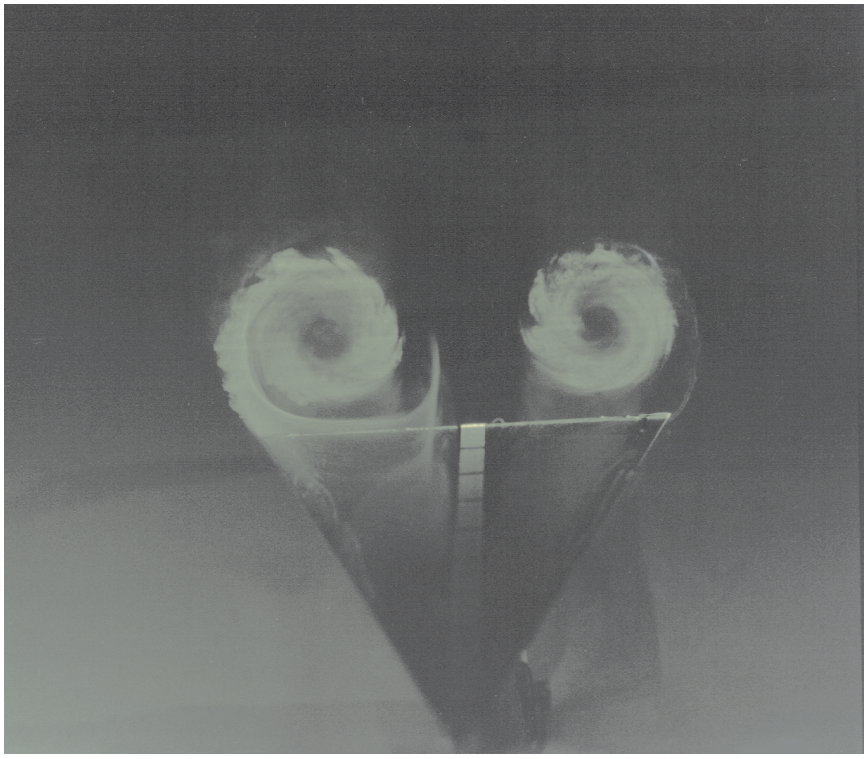

Figure 13.- Pulsed laser light sheet flow visualization of the vortex flow - unburst condition.

Figure 14.- Pulsed laser light sheet flow visualization of the vortex flow - burst condition.

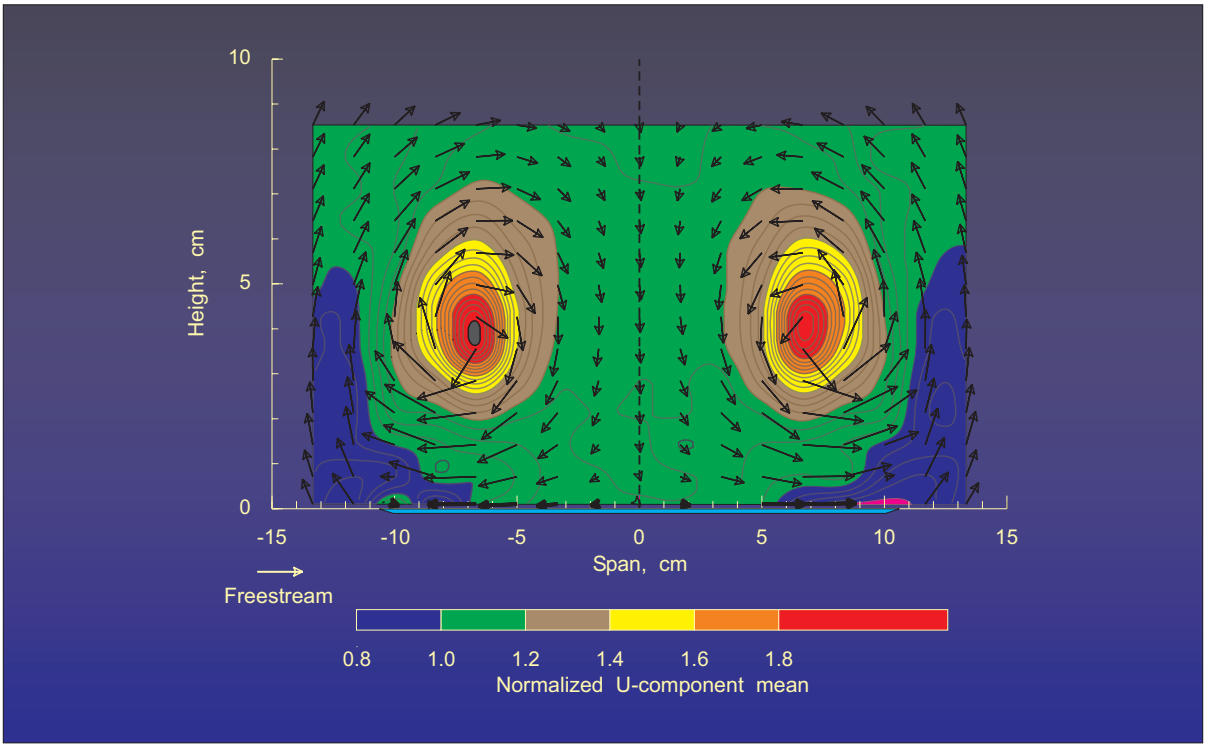

Figure 15.- Mean velocity measurements of the vortex flow above the 75^{o} delta wing at an angle of attack = 20.5^{o}.

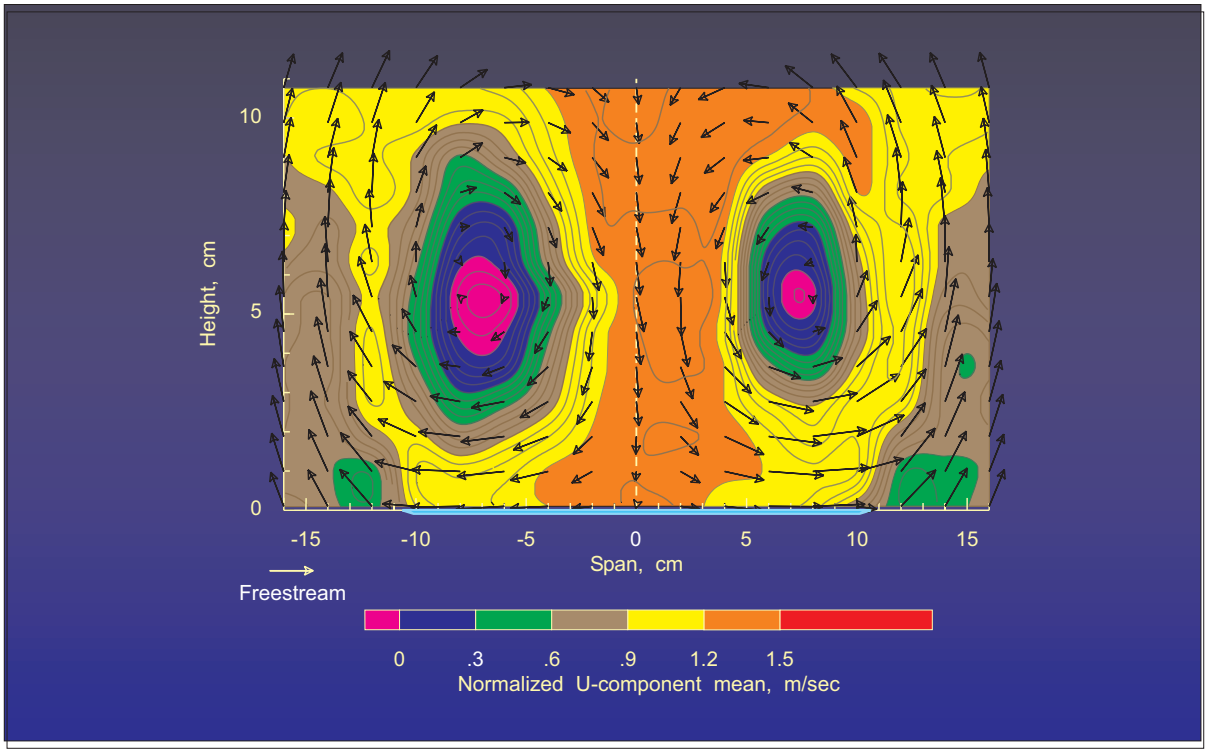

Figure 16.- Mean velocity measurements of the vortex flow above the 75^{o} delta wing at an angle of attack = 40.0^{o}.

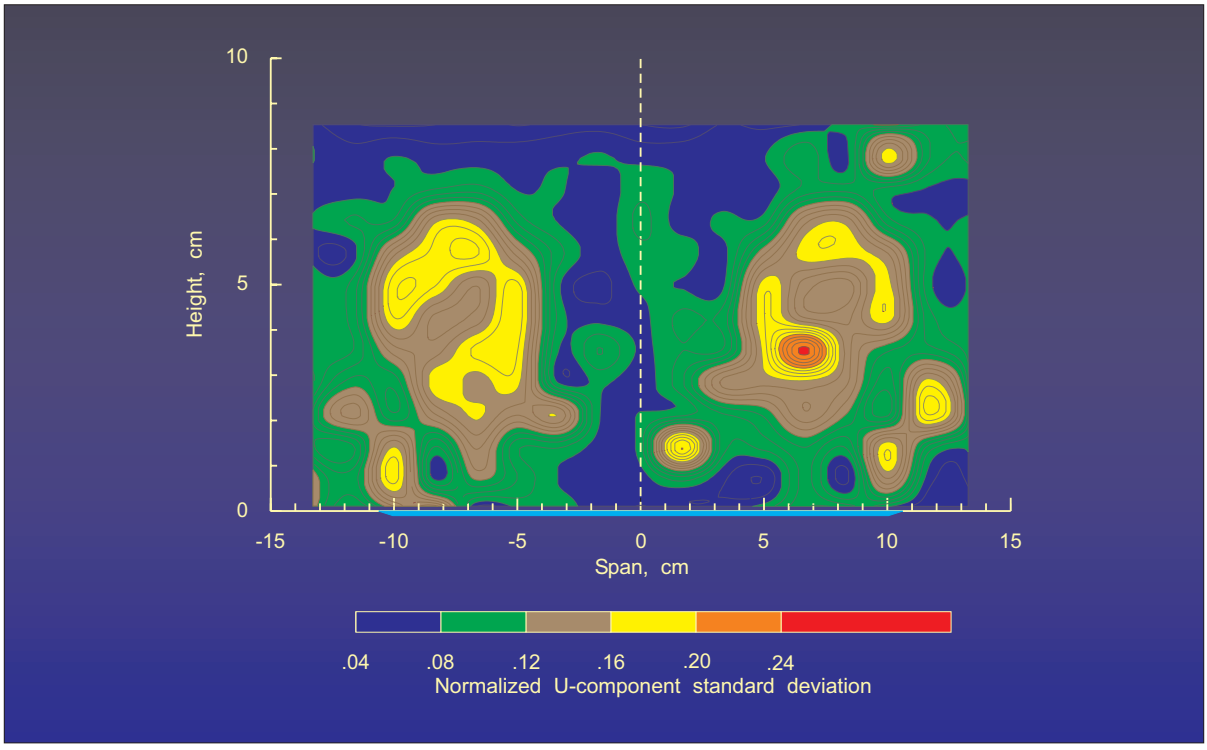

Figure 17.- Contours of streamwise normalized standard deviation of the vortex flow above the 75^{o} delta wing at an angle of attack = 20.5^{o}.

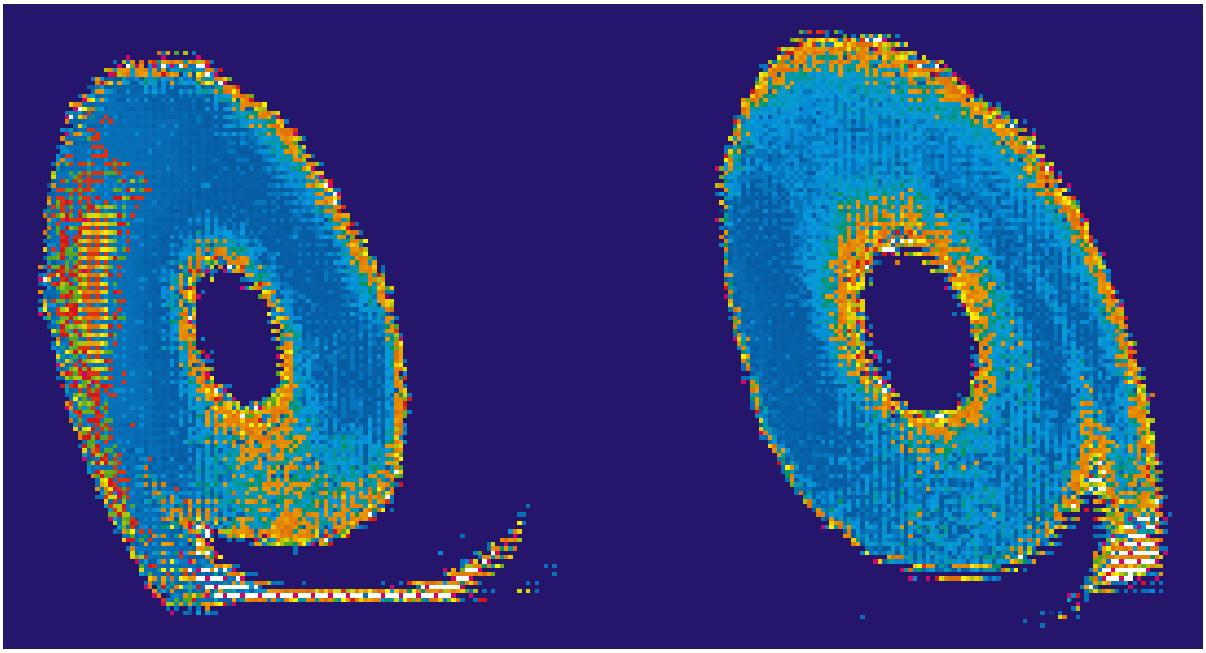

Figure 18.- Single frame DGV velocity contour map of the vortex flow field above a delta wing at 20.5^{o} angle of attack, velocity component is 26.5^{o} from the streamwise direction in the horizontal plane.

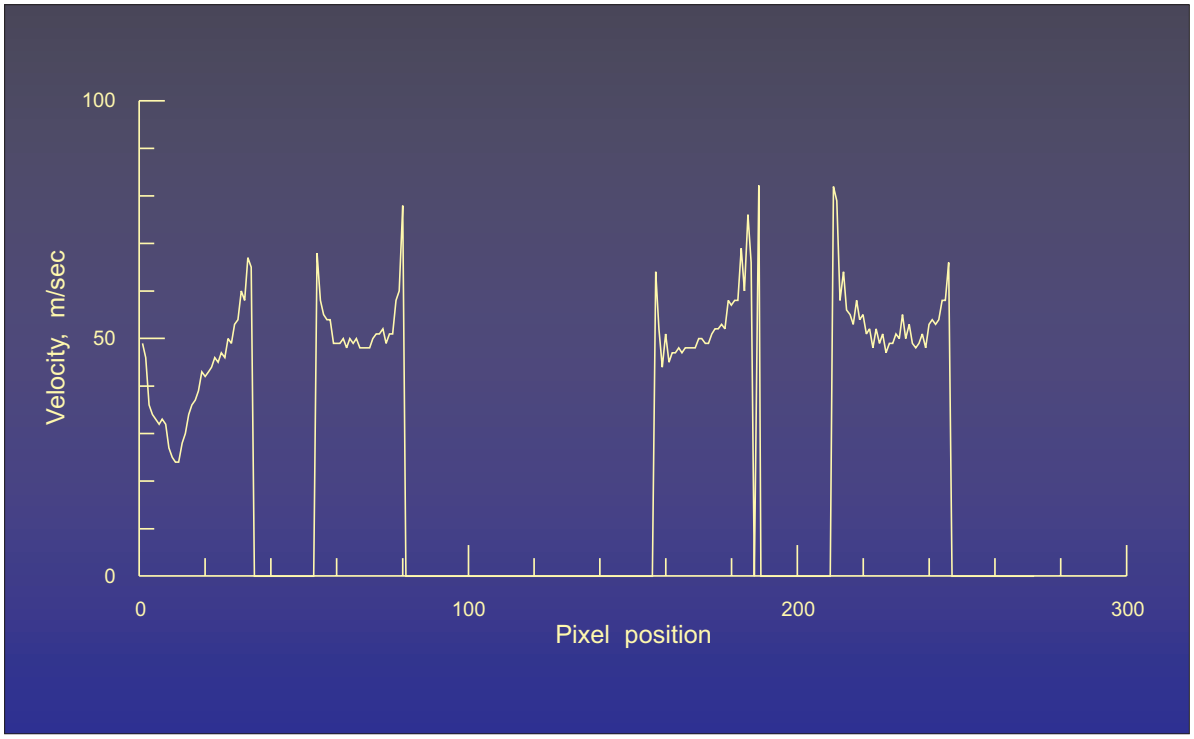

Figure 19.- Normalized signal amplitude along a horizontal line passing through the center of the vortices of the single frame DGV velocity map.

Figure 20.- Photograph of an F-18 fighter at high angle of attack.

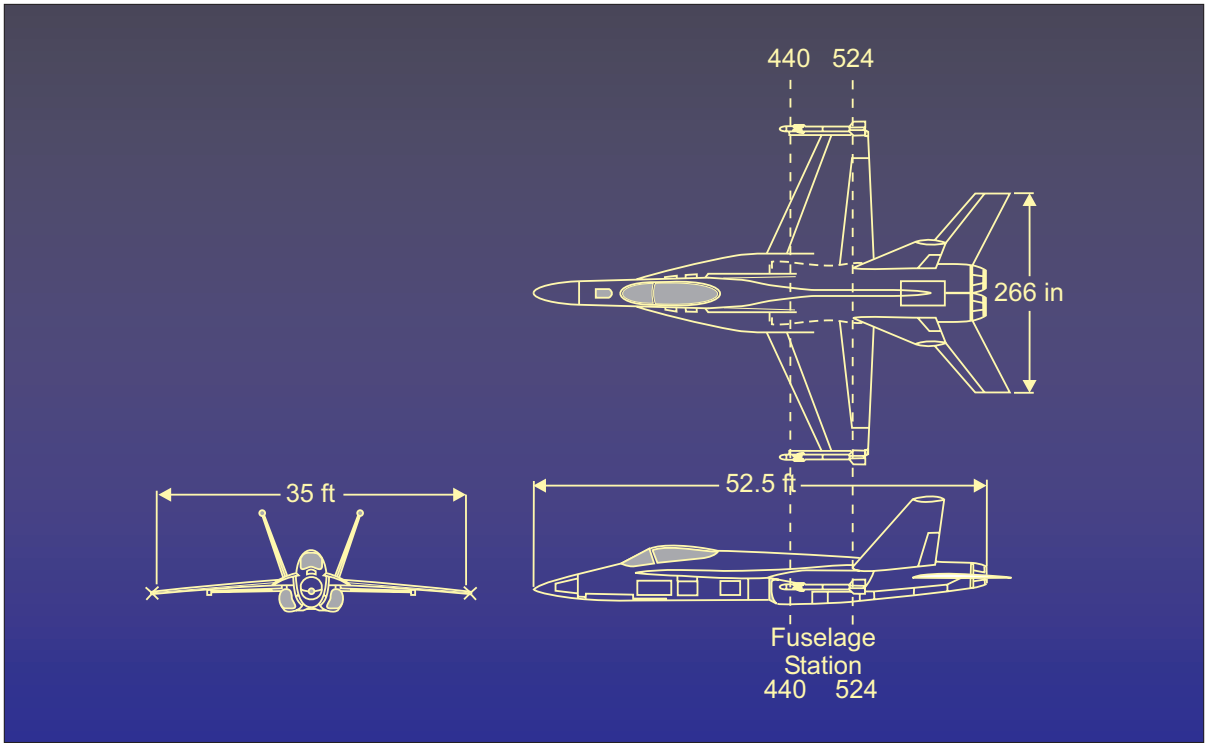

Figure 21.- Three-view diagram of the YF-17 configuration.

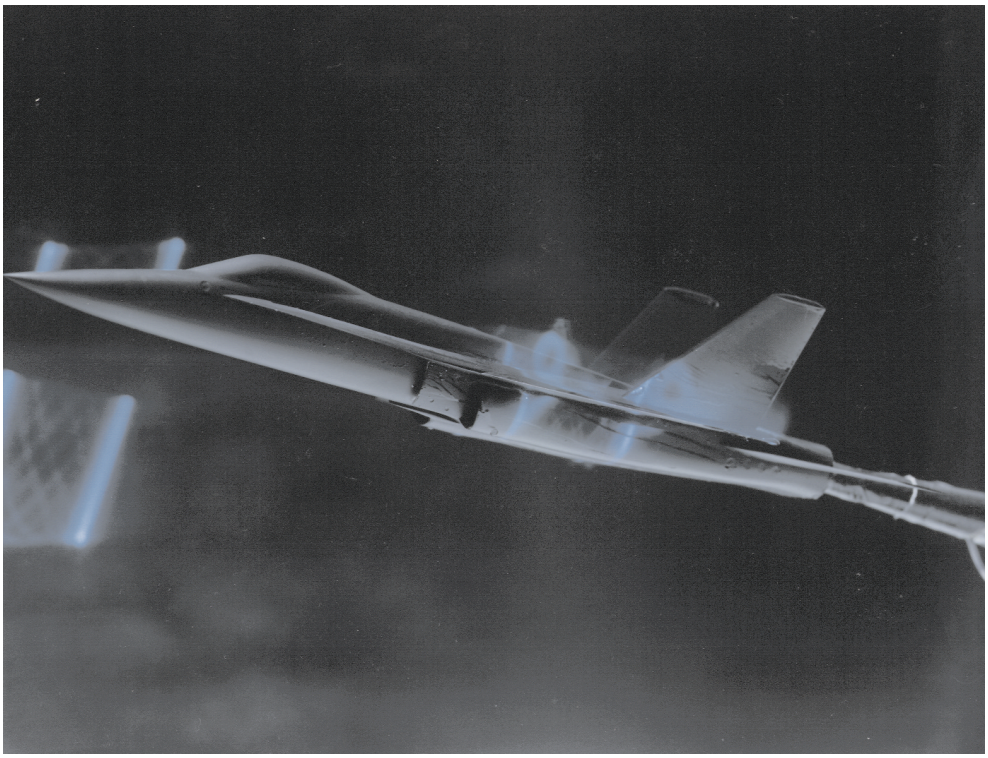

Figure 22.- Visualization of the vortical flow field above the YF-17 at stations 440 and 524 with the model set to an angle of attack = 15^{o}.

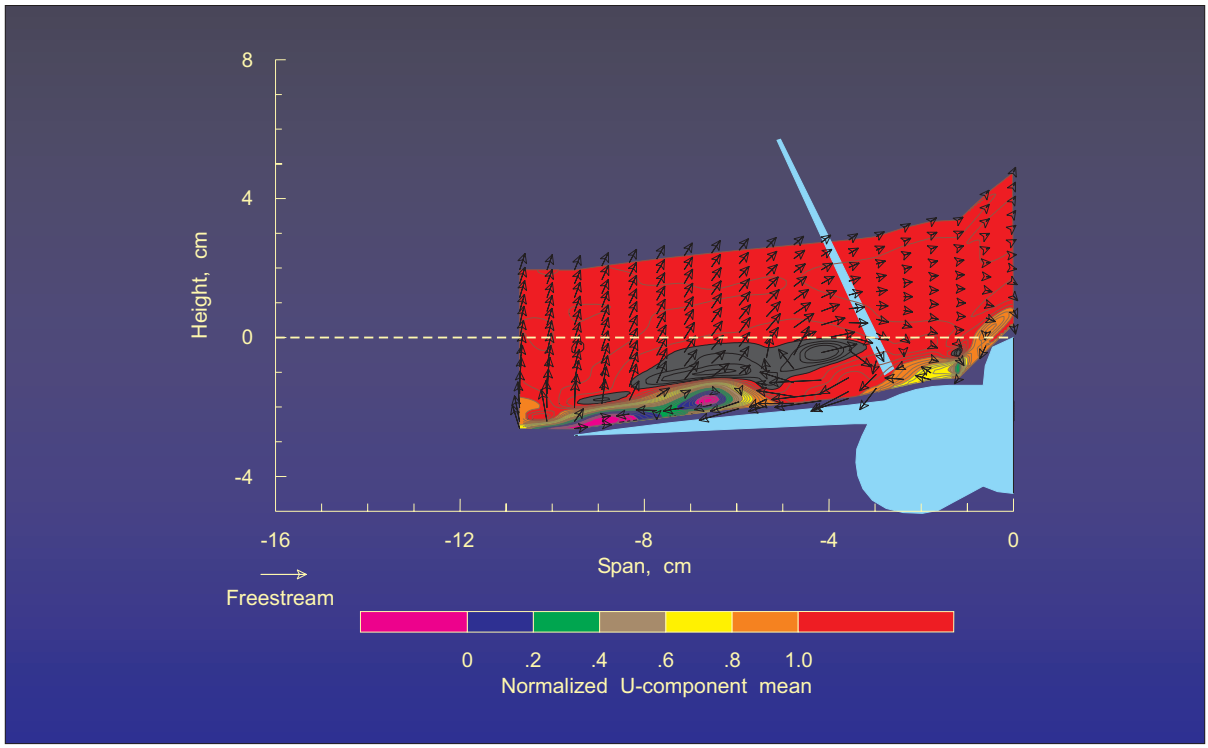

Figure 23.- Mean velocity measurements of the vortex flow above the YF-17 model at an angle of attack = 15^{o}, station 440.

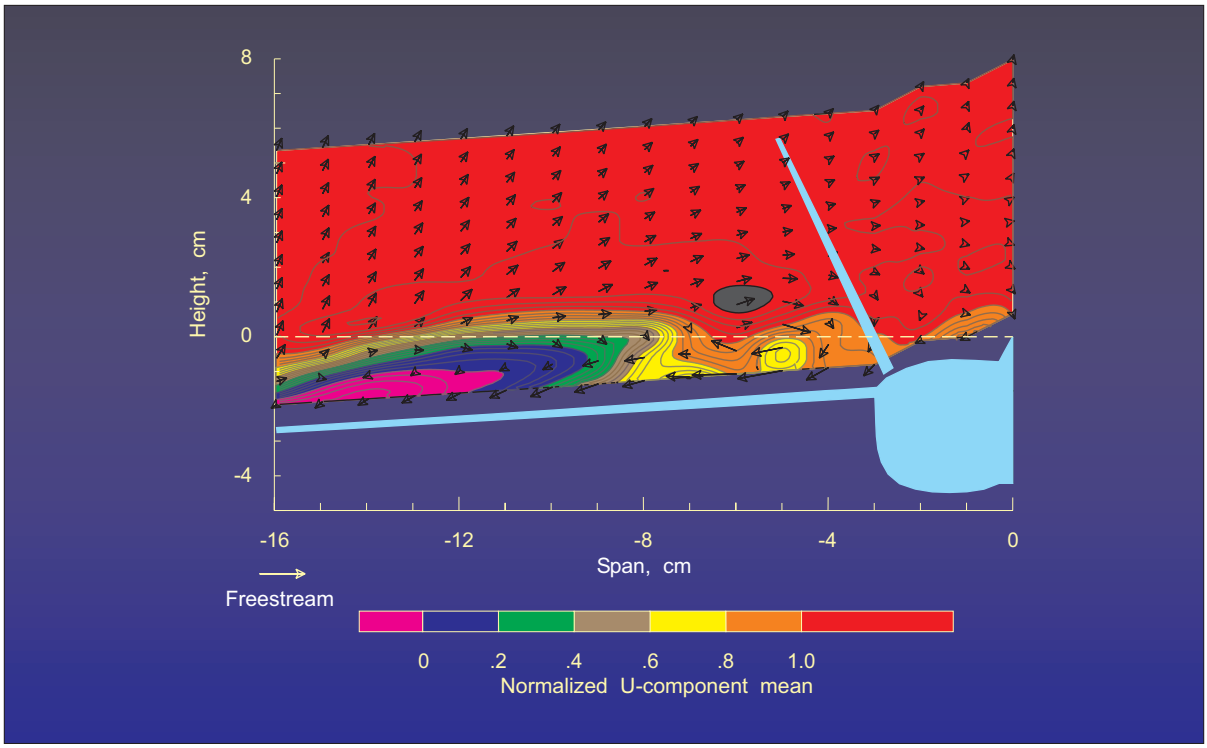

Figure 24.- Mean velocity measurements of the vortex flow above the YF-17 model at an angle of attack = 15^{o}, station 524.

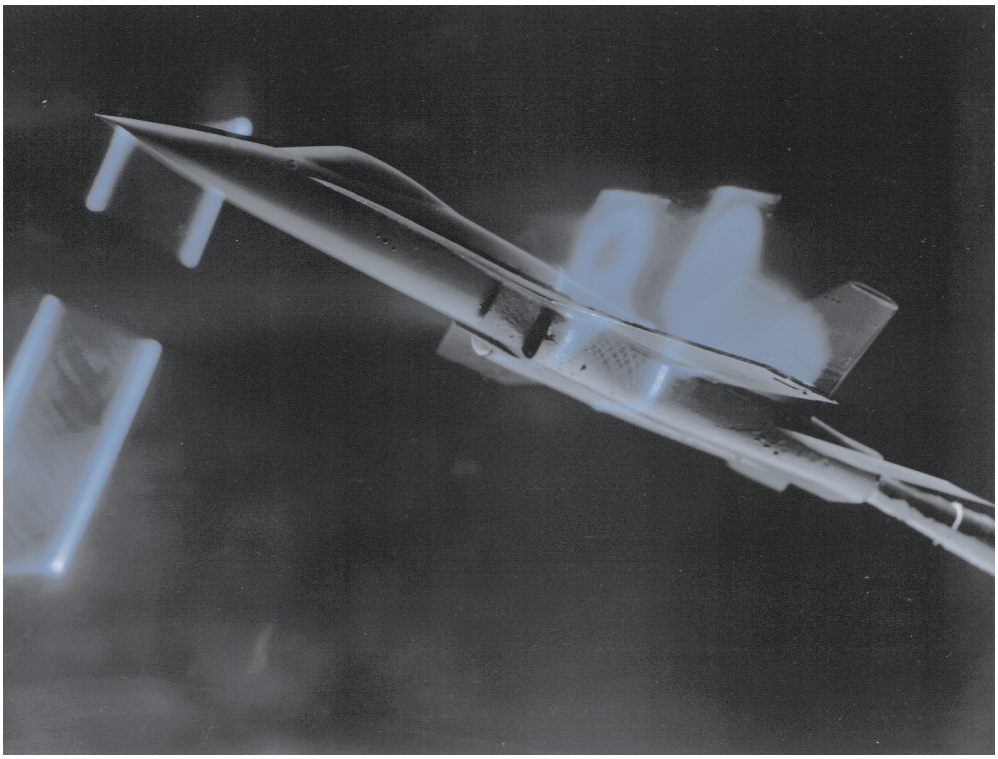

Figure 25.- Visualization of the vortical flow field above the YF-17 at stations 440 and 524 with the model set to an angle of attack = 25^{o}.

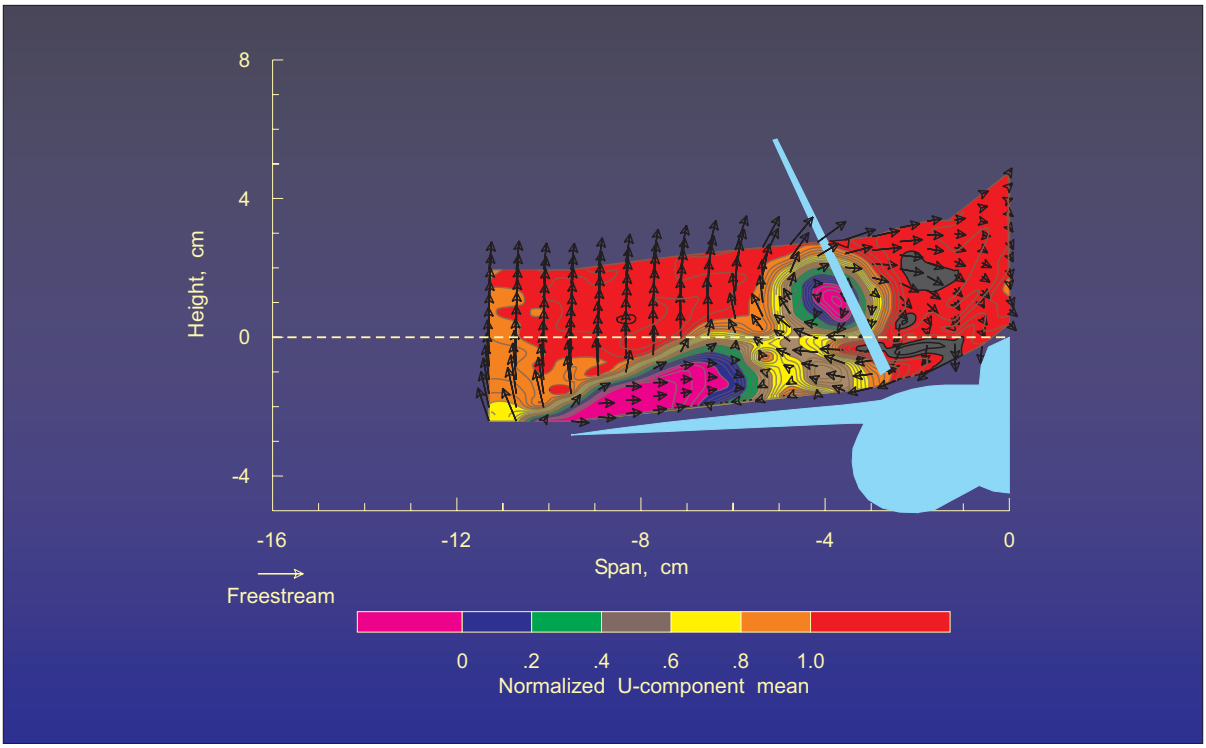

Figure 26.- Mean velocity measurements of the vortex flow above the YF-17 model at an angle of attack = 25^{o}, station 440.

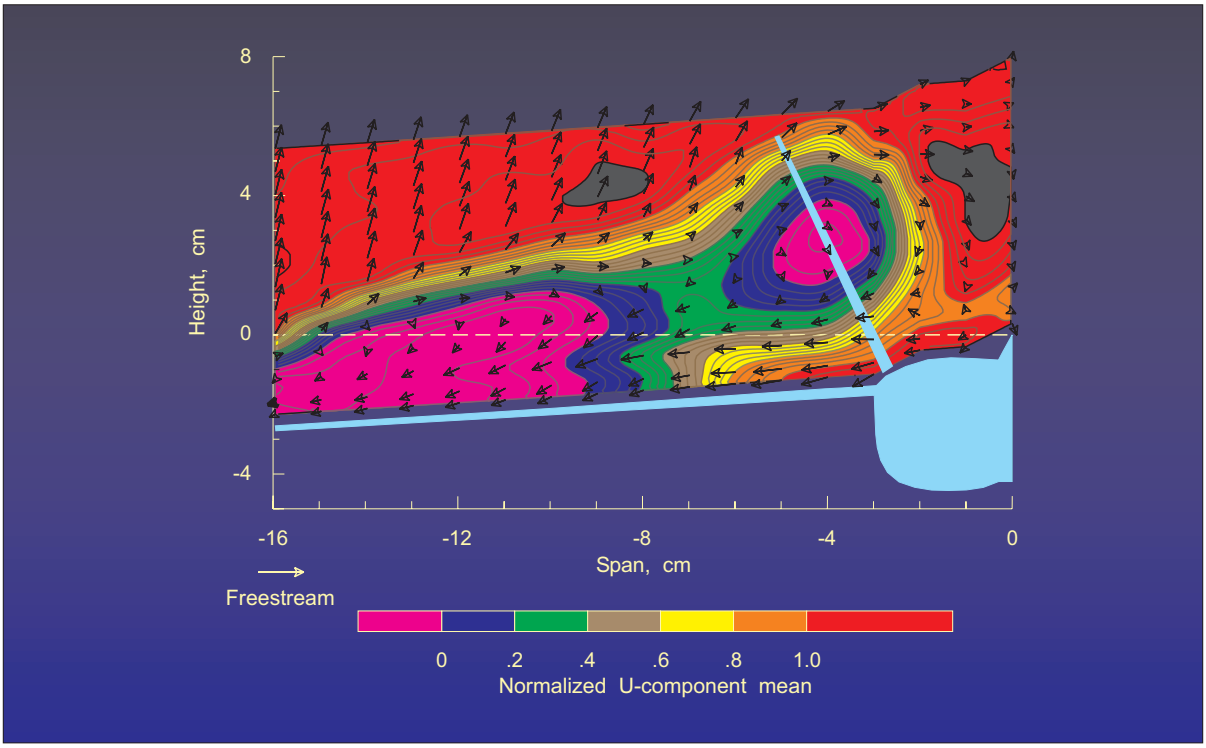

Figure 27.- Mean velocity measurements of the vortex flow above the YF-17 model at an angle of attack = 25^{o}, station 524.

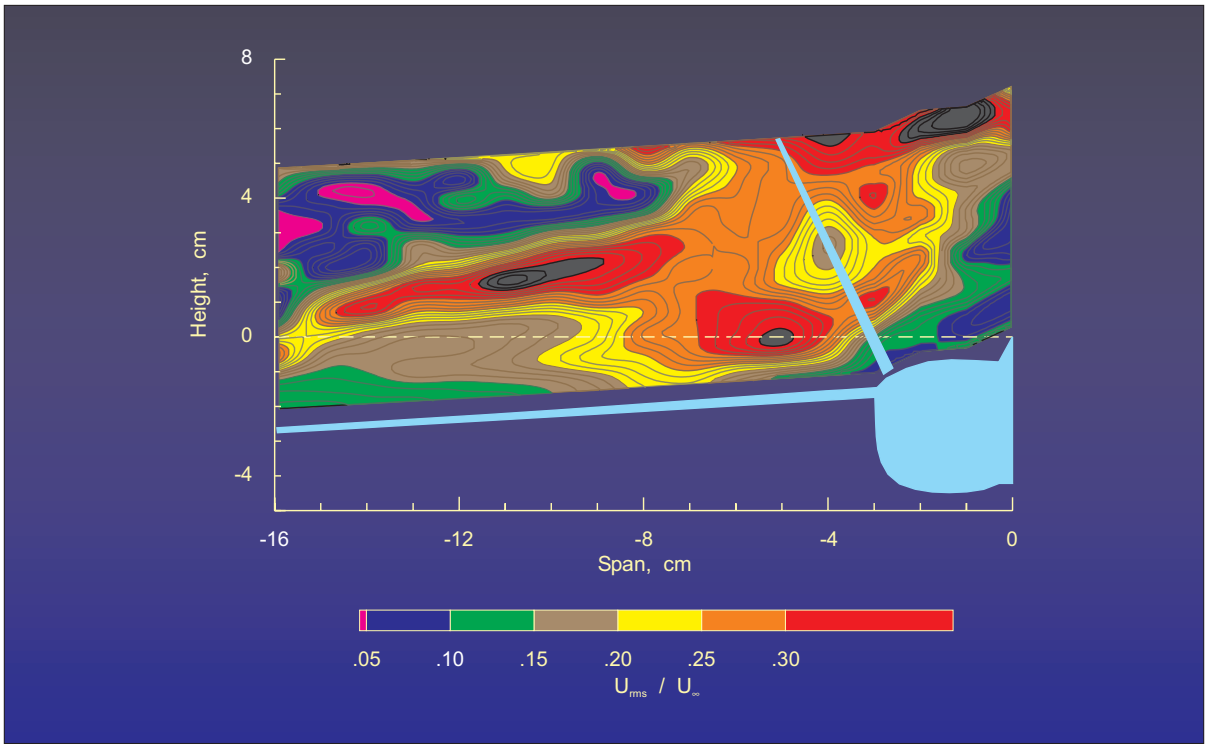

Figure 28.- Contours of streamwise normalized standard deviation of the vortex flow above the YF-17 model at an angle of attack = 25°, station 524.

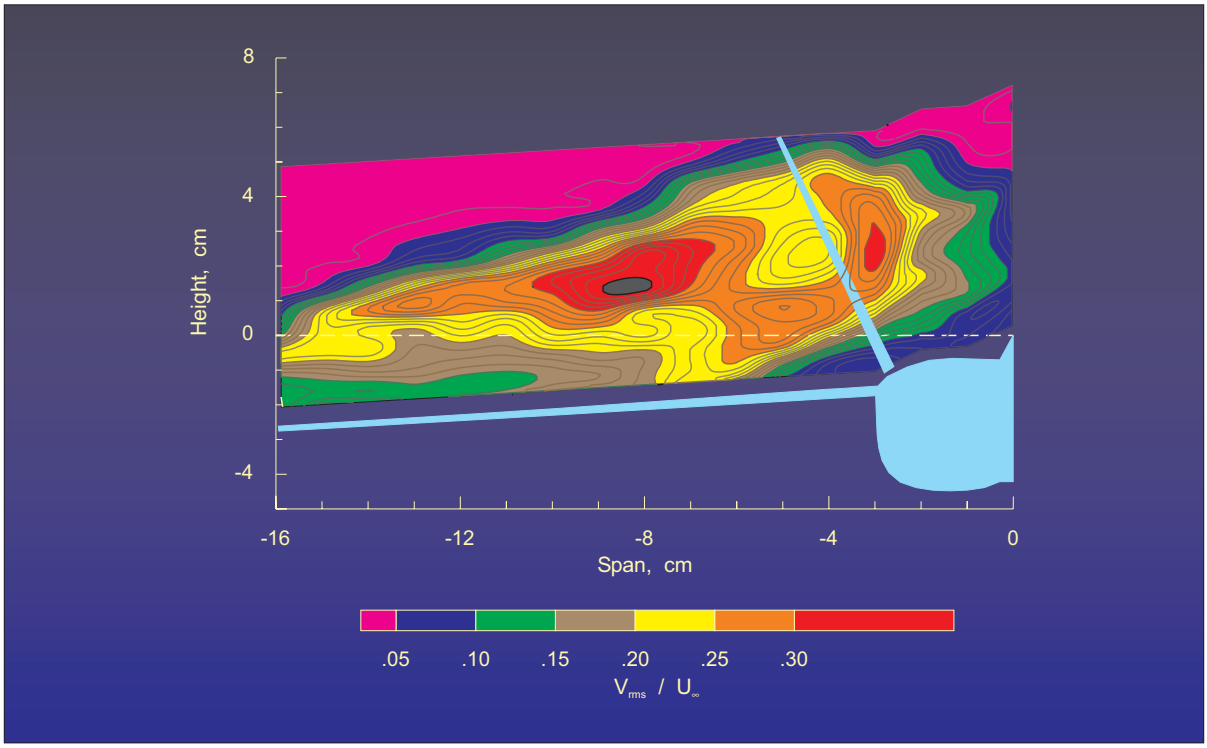

Figure 29.- Contours of vertical normalized standard deviation of the vortex flow above the YF-17 model at an angle of attack = 25°, station 524.

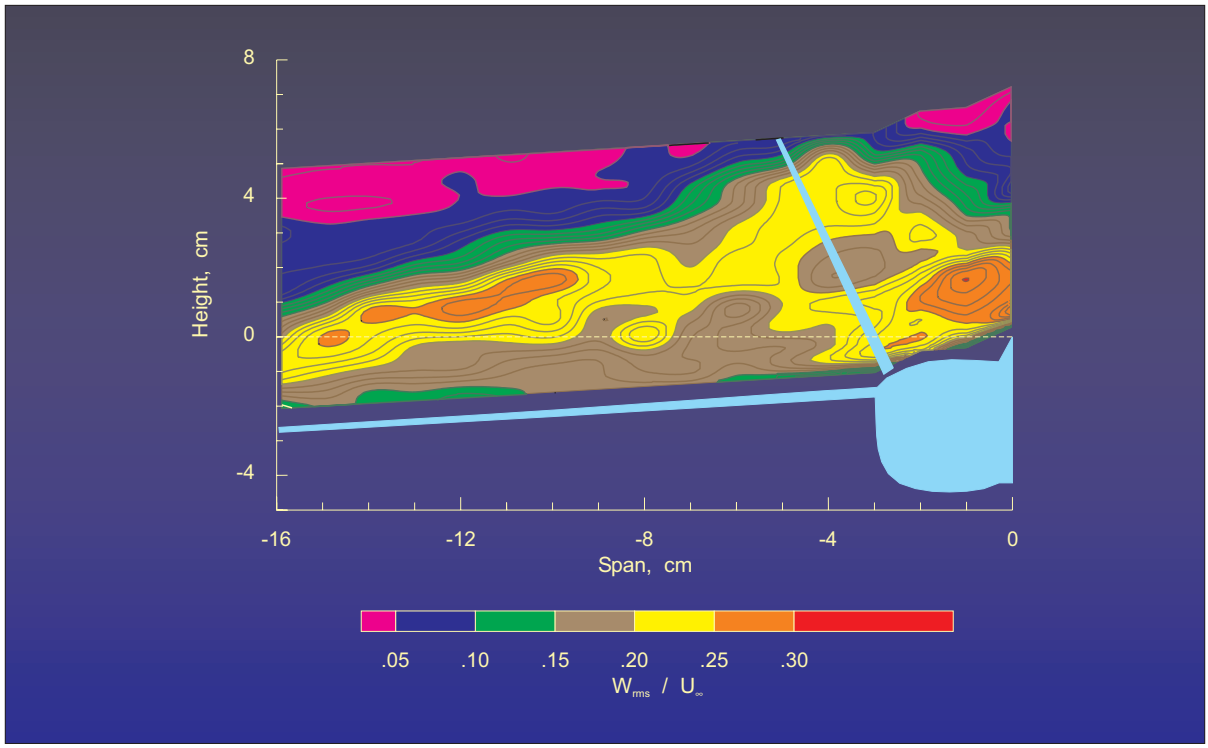

Figure 30.- Contours of traverse normalized standard deviation of the vortex flow above the YF-17 model at an angle of attack = 25^{o}, station 524.